JOURNAL OF GEOPHYSICAL RESEARCH, VOL. 112, B06208, doi:10.1029/2006JB004364, 2007

Thermodynamic properties of Mg_2SiO_4 liquid at ultra-high pressures from shock measurements to 200 GPa on forsterite and wadsleyite

Jed L. Mosenfelder,[1] Paul D. Asimow,[1] and Thomas J. Ahrens[1,2]

Received 24 February 2006; revised 22 November 2006; accepted 1 March 2007; published 30 June 2007.

[1] Polycrystalline samples of Mg_2SiO_4 forsterite and wadsleyite were synthesized and then dynamically loaded to pressures of 39–200 GPa. Differences in initial density and internal energy between these two phases lead to distinct Hugoniots, each characterized by multiple phase regimes. Transformation to the high-pressure phase assemblage MgO + $MgSiO_3$ perovksite is complete by 100 GPa for forsterite starting material but incomplete for wadsleyite. The datum for wadsleyite shocked to 136 GPa, however, is consistent with the assemblage MgO + $MgSiO_3$ post-perovksite. Marked increases in density along the Hugoniots of both phases between ~130 and 150 GPa are inconsistent with any known solid-solid phase transformation in the Mg_2SiO_4 system but can be explained by melting. Density increases upon melting are consistent with a similar density increase observed in the $MgSiO_3$ system. This implies that melts with compositions over the entire Mg/Si range likely for the mantle would be negatively or neutrally buoyant at conditions close to the core-mantle boundary, supporting the partial melt hypothesis to explain the occurrence of ultra-low velocity zones at the base of the mantle. From the energetic difference between the high-pressure segments of the two Hugoniots, we estimate a Grüneisen parameter (γ) of 2.6 ± 0.35 for Mg_2SiO_4-liquid between 150 and 200 GPa. Comparison to low-pressure data and fitting of the absolute pressures along the melt Hugoniots both require that γ for the melt increases with increasing density. Similar behavior was recently predicted in $MgSiO_3$ liquid via molecular dynamics simulations. This result changes estimates of the temperature profile, and hence the dynamics, of a deep terrestrial magma ocean.

Citation: Mosenfelder, J. L., P. D. Asimow, and T. J. Ahrens (2007), Thermodynamic properties of Mg_2SiO_4 liquid at ultra-high pressures from shock measurements to 200 GPa on forsterite and wadsleyite, *J. Geophys. Res.*, *112*, B06208, doi:10.1029/2006JB004364.

1. Introduction

[2] Evidence from mineral physics, geophysics, and cosmochemistry has now firmly established that perovskite-structured (Mg,Fe)SiO_3 and (Mg,Fe)O are the dominant solid phases present throughout the lower mantle [*Knittle and Jeanloz*, 1987; *Fiquet et al.*, 2000; *Shim et al.*, 2001b], up to pressures where a phase change to a post-perovskite phase (i.e., $CaIrO_3$ structure [*Murakami et al.*, 2004]) and/or melting [*Akins et al.*, 2004; *Stixrude and Karki*, 2005] occur at depths near the core-mantle boundary (CMB). Improved constraints on the thermodynamic properties of all of these phases are needed to improve our knowledge of phase equilibria in the lower mantle. In particular, little is known about the properties of melts that might exist in this region of the Earth [cf. *Stixrude and Karki*, 2005]; these data are crucial to understanding the consequences of such melting for mantle dynamics. Shock wave experiments provide the equation of state (EoS) at pressures and temperatures difficult to obtain using laser-heated diamond-anvil cells and serve to resolve discrepancies in melting behavior. Data over a wide range of pressures, extending into and beyond the conditions of the CMB (~136 GPa, ~4000 K), can be used to constrain the thermodynamic properties of very high pressure melts. One such property, the Grüneisen parameter (γ), can be accurately determined at very high compression by comparison of the principal Hugoniots of low-pressure phases and their presynthesized high-pressure equivalents [cf. *Luo et al.*, 2002], which obtain different internal energy states at equal volume upon shock loading. The γ of Mg_2SiO_4 liquid is also of particular importance for estimating the adiabatic temperature gradient in a terrestrial magma ocean [*Miller et al.*, 1991].

[3] Here we present the results of new shock wave experiments conducted using advanced recording techni-

[1]Division of Geological and Planetary Sciences, California Institute of Technology, Pasadena, California, USA.
[2]Lindhurst Laboratory of Experimental Geophysics, Seismological Laboratory, California Institute of Technology, Pasadena, California, USA.

0148-0227/07/2006JB004364$09.00

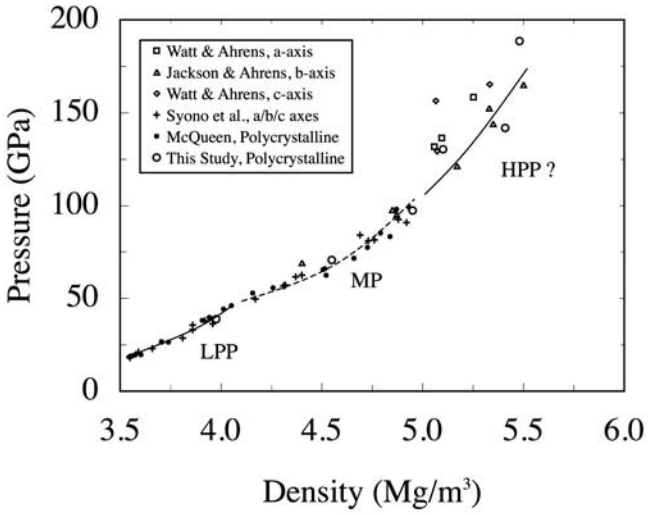

Figure 1. Selected pressure-density Hugoniot data for Mg_2SiO_4 forsterite. Previously interpreted phase regimes shown schematically with solid (LPP, HPP) and dashed (MP) curves (see text for abbreviations). Data on low-porosity polycrystalline samples from the work of *McQueen* [1968] (filled circles) and this study (open circles). Single-crystal data from the work of *Jackson and Ahrens* [1979] and *Watt and Ahrens* [1983] differentiated for crystallographic axis (squares, triangles and diamonds for *a*, *b*, and *c* axes, respectively). Single-crystal data from the work of *Syono et al.* [1981a] (cross symbols) not differentiated for crystallographic axis; only results from impedance match analysis shown.

ques at pressures up to 200 GPa on polycrystalline samples of Mg_2SiO_4 forsterite (Fo) and wadsleyite (one of the high-pressure polymorphs of forsterite). Although the shock compression behavior of Fo has been studied previously [*McQueen*, 1968; *Ahrens*, 1971; *Jackson and Ahrens*, 1979; *Raikes and Ahrens*, 1979; *Lyzenga and Ahrens*, 1980; *Syono et al.*, 1981a, 1981b; *Syono and Goto*, 1982; *Watt and Ahrens*, 1983], Hugoniot data on low-porosity polycrystalline samples are limited to pressures below 100 GPa [*McQueen*, 1968], and the data at higher pressures on single-crystal samples [*Jackson and Ahrens*, 1979; *Watt and Ahrens*, 1983] show considerable scatter (Figure 1). In static experiments above ~23 GPa [*Ito and Takahashi*, 1989; *Shim et al.*, 2001a; *Fei et al.*, 2004], Mg_2SiO_4 breaks down to form the assemblage MgO (periclase, Pe) + $MgSiO_3$ perovskite (Pv). Evidence from previous shock wave experiments suggests that the same transformation occurs during dynamic loading as well [*Jackson and Ahrens*, 1979; *Syono et al.*, 1981b], albeit at much higher pressures as a result of the overstepping of equilibrium boundaries necessary to achieve significant transformation on the short timescales of shock pressure risetimes.

[4] Melting must occur at some higher pressure along the Hugoniot of Mg_2SiO_4 forsterite, but the data are too discrepant among the various studies to resolve the pressure at which this occurs and the density change upon melting. Shock melting can be detected in at least three different ways: from a drop in shock temperature as a superheated solid gives way to liquid with increasing pressure, from a sharp decrease in sound velocity behind the shock front (resulting from wave travel at the bulk sound velocity in the liquid as opposed to the longitudinal sound velocity in the solid), and from changes in compressibility along the Hugoniot that cannot be explained by other phase changes. A coincidence of all three indicators at the same pressure is particularly strong evidence of melting. Melting on the Fo Hugoniot was not recognized in earlier studies [*Jackson and Ahrens*, 1979; *Lyzenga and Ahrens*, 1980; *Watt and Ahrens*, 1983]. However, for $Mg_{1.8}Fe_{0.2}SiO_4$ olivine (Fo90), melting was well defined at pressures between 143 and 150 GPa on the basis of all three of these indicators [*Furnish and Brown*, 1986; *Brown et al.*, 1987a, 1987b] and more recently was inferred for Fo at similar pressures on the basis of reinterpretation of shock wave temperature data [*Luo et al.*, 2004]. The measurement of sound speed in Fo90 liquid at 168 GPa by *Brown et al.* [1987b] and application of equation (10) in their paper also provides the only prior determination of the Grüneisen parameter of an olivine-composition liquid at such high pressures. Their value of 2.1 ± 0.1 is substantially larger than the value (~0.5) calculated from the thermodynamic properties of the liquid at ambient or low pressures (see section 4.2 for details of the calculation). An increase in γ with compression is unusual for solids but has been predicted recently for $MgSiO_3$ liquid on the basis of molecular dynamics simulations [*Stixrude and Karki*, 2005].

[5] There are no previous data on the shock compression behavior of wadsleyite, but we expect from the behavior of analogous low-density/high-density phase pairs in the $MgSiO_3$ [*Akins et al.*, 2004] and SiO_2 [*Lyzenga and Ahrens*, 1980; *Luo et al.*, 2002] systems that wadsleyite will shock to lower temperatures at given volume or pressure, and hence transformations to the high-pressure solid assemblage and melting may be delayed to higher pressure by kinetic and/or phase equilibrium considerations.

2. Experimental Methods

2.1. Sample Synthesis

[6] The forsterite samples were hot-pressed for 4 hours at nominal conditions of 3 GPa and 1573 K in an end-loaded piston-cylinder device, using 1.27 cm CaF_2 cell assemblies. The starting material was fine-grained synthetic forsterite powder (see the work of *Mosenfelder et al.* [2006] for details of the powder synthesis), which was inserted into a capsule made from rhenium foil. The assemblies were dried at ~500 K overnight prior to running in the press. Temperature was measured using type C thermocouples. A soft pressure medium (CaF_2 below the sample) and a schedule of simultaneous slow decompression (1 MPa/minute) and cooling (1 K/minute) were employed in order to inhibit cracking of the samples during recovery [cf. *Gwanmesia et al.*, 1993; *Farver et al.*, 1994]. One half of each recovered sample was retained for use in the shock wave experiments, while the other half was used as the starting material for subsequent wadsleyite synthesis, which was performed in a Walker multi-anvil device.

[7] The cell assemblies for the multi-anvil experiments consisted of 14 mm sintered, Cr-doped MgO octahedra with zirconia insulating sleeves and thin (4.0 mm outer diameter, 3.5 mm inner diameter) graphite sleeve furnaces, designed to yield a larger sample volume than our standard assem-

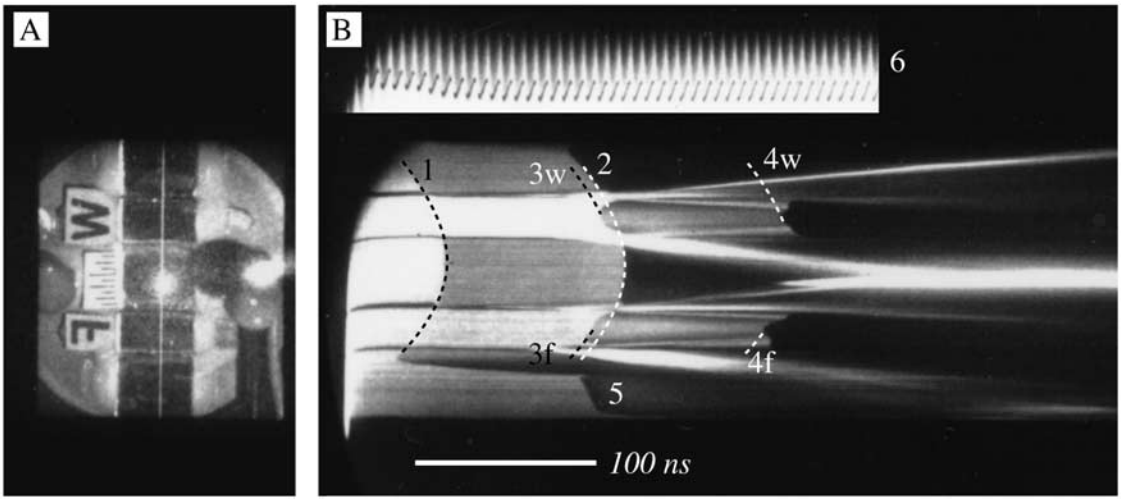

Figure 2. (a) Target image for shot 350, showing one mirror covering each sample and three mirrors on driver plate. White line represents slit position across sample filmed during shock event. Image is reversed on account of relay mirror. (b) Dynamic streak corresponding to static image. Features marked on streak are (1) first arrival on driver plate mirrors, (2) final arrival through front-sides of glass mirrors on driver plate (3w, 3f) first arrivals on mirrors covering wadsleyite and forsterite samples, respectively, (4w, 4f) final arrivals on sample mirrors, (5) edge effect due to misalignment of driver plate with respect to projectile, (6) superimposed portion of radio-frequency modulated streak used for time calibration, showing modulated signal every 6.595 ns. Also shown, 100 ns scale bar.

blies [*Mosenfelder et al.*, 2006]. The starting material for each experiment was inserted into a Re foil capsule. The assemblies were dried overnight at 525 K prior to running. Compression was achieved with 8-mm truncation-edge-length Toshiba WC anvils and pyrophyllite gaskets, backed up by paper and Teflon tape for support and electrical insulation. Temperature was measured using axial type C thermocouples, uncorrected for the effect of pressure on emf. A multistage, computer-controlled decompression and cooling path [cf. *Gwanmesia et al.*, 1993], along with the use of a NaCl disk below the samples, served to inhibit cracking during decompression. The syntheses were run at 770 metric tons and 1373 K, for 4 hours. The duration of the experiments was chosen to ensure complete transformation, according to available kinetic data for the transformation of forsterite to wadsleyite [*Mosenfelder et al.*, 2001; *Kubo et al.*, 2004]. The estimated pressure at 770 metric tons is 15 GPa but is beyond the range of our calibration for the 14/8 assembly [*Mosenfelder et al.*, 2006] and hence has an uncertainty of about ±1 GPa. Note that even though graphite is metastable at these conditions, the furnaces performed well throughout the experiments as a consequence of the slow kinetics of transformation to diamond [*Gwanmesia et al.*, 1993].

[8] The recovered forsterite and wadsleyite samples were comprised of cylinders typically 3.3 mm in diameter, from which the Re foil capsule was removed. We used bulk density measurement (via Archimedes' method using immersion in toluene), X-ray diffraction (XRD), scanning electron microscopy (SEM), and Raman spectroscopy to characterize the samples. Bulk densities (ρ_0) were 3.22 ± 0.02 Mg/m^3 for forsterite ($\ll$1% effective porosity, compared with a theoretical density of 3.227 Mg/m^3) and 3.41 ± 0.02 Mg/m^3 for wadsleyite (1–2% effective porosity, compared with a theoretical density of 3.47 Mg/m^3). The density deficit for wadsleyite samples could reflect incomplete transformation during the synthesis, but relict forsterite was not detected using XRD or Raman spectroscopy. The forsterite polycrystals exhibited an equilibrium foam grain-boundary microstructure, with a grain size ranging from ~10 to 200 μm. The average grain size of the wadsleyite samples was finer, presumably as a result of transformation and slower grain growth kinetics at the lower synthesis temperature. Impurities (<1%) detected using energy-dispersive analysis on the SEM include NaCl, CaF_2, enstatite, and diopside.

2.2. Shock Compression Experiments

[9] Doubly polished disks (lapped to within ±0.003 mm of uniform thickness) with dimensions of ~3.3-mm diameter and ~1-mm thickness were prepared from the samples and two disks (one of each phase) were mounted onto metal (W, Al 1100, Ti or Ta) driver plates (Figure 2) for each planar shock wave experiment (Table 1). The samples and driver plate were covered with an array of glass mirrors, aluminized on the contact side. In the case of shot 1060, we used the inclined-mirror method [*Vassiliou and Ahrens*, 1982] to distinguish the arrivals of the elastic and plastic waves through the front of the samples. In this case, each sample was covered with one flat and one inclined mirror.

[10] The experiments were performed either in a 90/25-mm two-stage light-gas gun or in a 40-mm propellant gun (for shot 1060). Plastic projectiles bearing metal flyer plates of the same composition as the driver plates were accelerated to velocities (u_{fp}) of 1.96–6.86 km/s, measured

Table 1. Shock Experimental Parameters and Results[a]

Shot No.	Flyer-Driver Material	U_{fp}, km/s	ρ_0, Mg/m^3	U_s, km/s	u_p, km/s	P, Gpa	ρ, Mg/m^3	State[b]
Forsterite								
1060	W	1.96	3.22	7.97(0.12)	1.52(0.01)	38.9(0.6)	3.98(0.03)	LPP
347	Al 1100	5.37	3.25	8.71(0.10)	2.50(0.02)	70.6(0.6)	4.55(0.04)	MP
352	Ti	6.07	3.20	9.28(0.8)	3.28(0.02)	97.4(0.8)	4.95(0.04)	HPP
348	Ta	5.36	3.22	10.48(0.11)	3.87(0.02)	130.4(1.3)	5.10(0.05)	HPP
349	Ta	5.82	3.21	10.42(0.30)	4.23(0.03)	141.7(3.3)	5.41(0.13)	Melt
350	Ta	6.86	3.22	11.91 (0.13)	4.91 (0.02)	188.5 (2.0)	5.48(0.6)	Melt
Wadsleyite								
1060	W	1.96	3.37	8.15(0.13)	1.50(0.01)	41.1(0.6)	4.13(0.03)	LPP
347	Al 1100	5.37	3.42	9.36(0.12)	2.36(0.02)	75.5(0.6)	4.57(0.04)	LPP
352	Ti	6.07	3.41	10.04(0.09)	3.10(0.02)	106.2(0.8)	4.93(0.04)	MP
348	Ta	5.36	3.41	10.47(0.10)	3.82(0.02)	136.2(1.3)	5.36(0.05)	HPP
349	Ta	5.82	3.44	10.61(0.16)	4.16(0.02)	150.6(1.9)	5.61(0.07)	Melt
350	Ta	6.86	3.42	12.11(0.14)	4.83(0.02)	199.9(2.1)	5.68(0.06)	Melt

[a]Uncertainties denoted in parentheses; uncertainties in U_{fp} and ρ_0 are 0.01 km/s and 0.02 g/cm^3, respectively.
[b]Interpreted state on Hugoniot. LPP = Low pressure phase; MP = mixed-phase state; HPP = high-pressure phase assemblage.

by the double-flash X-ray method [*Jackson and Ahrens*, 1979]. Shock wave velocities (U_s) in the two samples were measured by filming the extinction of the glass mirrors with a streak camera writing over a duration of 660–670 ns (Figure 2). The camera writing rate is calibrated using a test streak modulated by a high-precision radio-frequency tuner at 151.6247 MHz, which provides a time signal every 6.595 ns and allows us to take into account nonlinearity of the camera writing rate. At this writing rate, the resolution of the film is better than 1 ns for clearly defined mirror cut-offs. The streak records were corrected for tilt and bowing of the flyer by fitting polynomial curves to the mirror extinctions [cf. *Mitchell and Nellis*, 1981a]. Particle velocity (u_p), pressure (P_H), and density (ρ_H) of the shock state were determined from impedance matching and the Rankine-Hugoniot equations (see section 3.1 below), using available standard Hugoniot data for the metal flyer and driver plates [*Marsh*, 1980; *Mitchell and Nellis*, 1981b; *Hixson and Fritz*, 1992]. Uncertainties in all derived parameters were obtained from uncertainties in the measured and standard quantities by analytical error propagation [cf. *Jackson and Ahrens*, 1979].

3. Calculation of Theoretical Hugoniots

[11] The phase(s) obtained at peak conditions in shock wave experiments are not normally observed directly. Therefore interpretation of shock wave data where phase transitions are expected depends on comparison of data to model calculations for proposed high-pressure phase assemblages. We use Mie-Grüneisen theory and third-order Birch-Murnaghan isentropes for these calculations, as summarized here.

3.1. The Rankine-Hugoniot Equations and Impedance Matching

[12] The measured quantities in a shock wave EoS experiment are initial density ρ_o, flyer velocity u_{fp}, sample thickness d, and shock traveltime t. Shock propagation velocity $U_s = d / t$. The flyer and driver plates are made of a standard material of initial measured density ρ_o^{fp}, the Hugoniot EoS of which ($U_s^{fp} = C_o^{fp} + s^{fp} u_p^{fp}$, where u_p is particle velocity, see also section 3.2 below) is known from previous measurements. For a shock propagating into a material initially at rest and at 0 pressure, conservation of mass, momentum, and energy are expressed:

$$\rho_H(U_s - u_p) = \rho_o U_s \tag{1}$$

$$P_H = \rho_o U_s u_p \tag{2}$$

$$\Delta E_H = \frac{P_H}{2}\left(\frac{1}{\rho_o} - \frac{1}{\rho_H}\right). \tag{3}$$

The requirements of continuity of velocity and stress across the flyer-driver and driver-sample interfaces, together with equations (1) and (2), lead to the impedance match solution for u_p:

$$s^{fp}\rho_o^{fp}(u_p)^2 - \left[\rho_o^{fp}\left(C_o^{fp} + 2s^{fp}u_{fp}\right) + \rho_o U_s\right] \cdot u_p + \rho_o^{fp}u_{fp}\left(C_o^{fp} + s^{fp}u_{fp}\right) = 0, \tag{4}$$

which always yields one physically reasonable quadratic solution [*Ahrens*, 1987].

3.2. Hugoniot EoS in the Absence of a Phase Transition

[13] A fully dense starting material with an initial density ρ_o, isentropic bulk modulus at 0 pressure K_{oS}, and pressure derivative of the bulk modulus K_S' has a plastic Hugoniot given to third order by $U_S = C_o + su_p$, where $C_o^2 = K_{oS} / \rho_o$ and $s = (K_S' + 1) / 4$ [*Ruoff*, 1967]. The U_s-u_p line can be converted to a P-ρ curve using equations (1) and (2) [e.g., *Ahrens*, 1987]. Hugoniot states beyond the Hugoniot Elastic Limit (HEL) for materials for which the isentropic EoS is known and for materials that experience no phase transitions on compression are expected to yield states given by these equations, although terms beyond third order become significant at high finite strains and may lead to differences on the order of 20% between s and $(K_S' + 1) / 4$ [*Steinberg*, 1982; *Jeanloz*, 1989].

3.3. Computed Hugoniots Considering Phase Transitions and/or Initial Porosity

[14] If the starting material differs in phase or density from the reference isentrope of the proposed assemblage

achieved at peak shock conditions, we use the following procedure. The reference isentrope of the high-pressure phase assemblage is defined by parameters ρ_{ref}, K_{oS} and K_S' and is given by a third-order Birch-Murnaghan expression:

$$P_s = 3K_{oS} f(2f+1)^{5/2}\left(1+\frac{3}{2}\left[K_s'-4\right]f\right), \quad (5)$$

where $f = [(\rho_H/\rho_{ref})^{(2/3)} - 1] / 2$, and the energy change due to compression along this isentrope is

$$\Delta E_S = \frac{9}{2}\frac{K_{oS}}{\rho_{ref}}\left(f^2 + \left[K_S'-4\right]f^3\right). \quad (6)$$

The Mie-Grüneisen form for the thermal pressure assumes that the Grüneisen parameter of the high-pressure assemblage is only a function of density, such that the energy difference between the reference isentrope and the Hugoniot state at equal density is given by

$$\Delta E_V = \frac{P_H - P_S}{\rho_H \gamma(\rho)}. \quad (7)$$

We define the Grüneisen parameter of a given material by a two-parameter function of density

$$\gamma(\rho) = \gamma_0[\rho/\rho_{ref}]^q. \quad (8)$$

Finally, accounting for the energy of transition ΔE_{tr} from the starting phase assemblage to the high-pressure phase assemblage at ambient pressure and temperature (taken as the difference in enthalpy of formation between the assemblages) and for the fact that internal energy is a path-independent state variable, we have

$$\Delta E_H = \Delta E_{tr} + \Delta E_S + \Delta E_V. \quad (9)$$

Note that the initial density of the target ρ_o [in equations (1), (2), and (4)] is not necessarily equal to ρ_{ref} even in the absence of phase changes; in the cases considered here, this accounts for initial porosity in the target. Equations (1)–(9) provide a closed-form solution as a function of density ρ_H for the expected Hugoniot state (i.e., P_H, ΔE_H, U_s, and u_p) of a starting material in some known phase at bulk initial density ρ_o driven to a candidate high-pressure phase assemblage defined by six parameters (ρ_{ref}, K_{oS}, K_S', γ_o, q, and ΔE_{tr}).

[15] Finally, if we wish to infer the temperature T_H of this model shock state, we also need to define the isochoric heat capacity C_V of the high-pressure phase assemblage and use the equations

$$T_S = T_o \exp\left\{\int_{P_H}^{\rho_{ref}} \rho\gamma(\rho)d(1/\rho)\right\} \quad (10)$$

$$\Delta E_V = \int_{T_S}^{T_H} C_V(T,\rho)\mathrm{d}T, \quad (11)$$

where C_V may be taken as a constant or, for more precise characterization, a Debye form may be used with parameters C_{vm} and θ_o [see *Luo et al.*, 2004].

4. Results and Discussion

[16] Six pairs of samples were dynamically compressed. Figure 2 shows a typical streak film record, demonstrating the time resolution of the streak camera and the typical curvature of the mirror cutoffs due to bowing of the flyer. The inclined mirror cutoffs for shot 1060 did not yield the anticipated two-wave structure information. In the case of wadsleyite, only one inclined streak was seen on the inclined mirror. This indicates that the elastic wave was overtaken by the plastic wave, enabling a clean cutoff corresponding to the plastic wave to be measured. For the forsterite sample, the arrival of an elastic precursor shortly before the plastic wave is suggested by the fuzziness of the cutoff on the flat mirror streak, which is similar to phenomena seen by *Ahrens* [1971] at comparable velocities for polycrystalline forsterite samples with higher porosity. In this case, the plastic wave velocity was estimated by measuring the final cutoff on the flat mirror. Interpretation of the mirror cutoffs for samples impacted at higher velocities is more straightforward because the HEL was far exceeded in these experiments [*Syono et al.*, 1981a].

4.1. Hugoniot Regimes

[17] The results are shown in Table 1 and in U_s-u_p and P-ρ space in Figure 3a and 3b, respectively. The Hugoniot of each starting material exhibits multiple regimes characterized by (1) elastic shock; (2) dynamic yielding and plastic Hugoniot of the low-pressure phase (LPP); (3) a "mixed-phase" (MP) region, indicating progressive transformation to a high-pressure solid phase assemblage; (4) a high-pressure phase (HPP) region; and (5) melting. The complexity of the region below the HEL [*Syono et al.*, 1981a; *Watt and Ahrens*, 1983], not studied in the present work, is not shown in Figure 3. In Figure 3, we show our preferred models for segmentation of each Hugoniot into these regimes. Figure 4 expands on the uncertainty in fitting model Hugoniots for the LPP and HPP regimes that results from considering a range of input parameters, specified below and in Table 2.

4.1.1. Low-Pressure Phase Plastic Regime

[18] Hugoniot states beyond the HEL that remain in the starting phase can be evaluated by reference to previous shock EoS experiments, where available, and/or by reference to EoS data from Brillouin scattering, static compression P-V-T, and/or ultrasonic experiments.

[19] Our datum for forsterite at ~40 GPa is consistent with previous experiments on both single crystal and polycrystalline forsterite that were interpreted by *Syono et al.* [1981a] as forsterite in a metastable LPP regime up to ~50 GPa. We note, however, that the best fitting LPP forsterite Hugoniot, $U_S = 6.43 + 1.06\ u_p$ (fitted to all data in the range $0.825 \le u_p \le 1.86$ km/s from the works of *Syono et al.* [1981a] and *McQueen* [1968]) implies K_{oS} = 133 GPa and $K_S' = 3.25$, which is inconsistent with the EoS of forsterite determined by recent static compression, Brillouin scattering, and ultrasonic studies (K_{oS} = 125–129 GPa and K_S' = 4.2–4.44 [*Andrault et al.*, 1995; *Duffy et al.*,

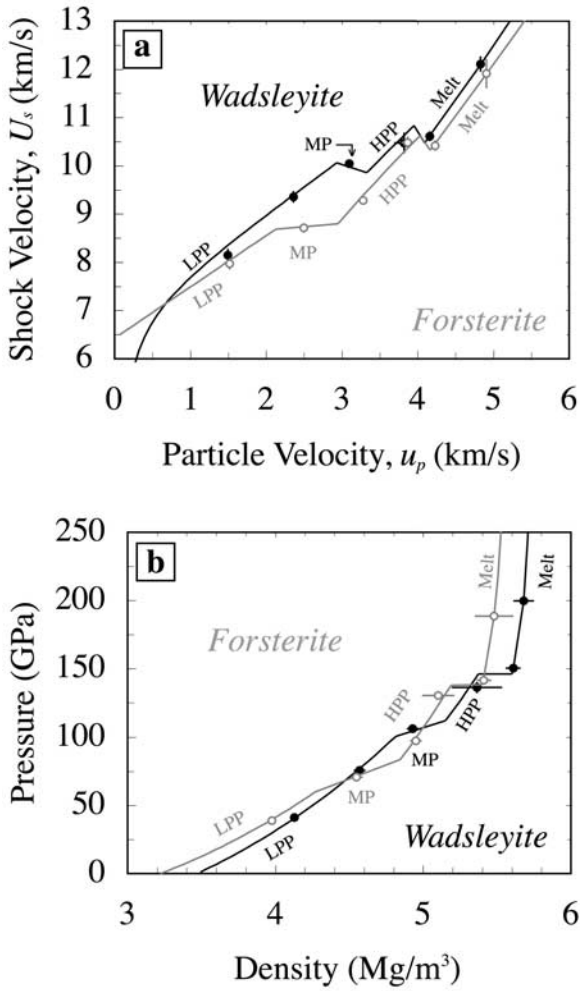

Figure 3. Hugoniot data for forsterite (open circles) and wadsleyite (closed circles) and preferred models from this study. Interpolated Hugoniots are shown by the heavy line for wadsleyite and light line for forsterite, divided into interpreted phase regimes (see text for abbreviations) (a) Shock velocity versus particle velocity. Uncertainties in particle velocity are smaller than symbol size. (b) Pressure versus density. Uncertainties in pressure for most experiments are smaller than the symbol size.

1995; *Downs et al.*, 1996; *Li et al.*, 1998; *Zhang*, 1998]). This discrepancy may be caused by residual strength effects above the HEL or by the onset of a mixed-phase regime at lower pressure than previously inferred. Alternatively, it may be an example of deviation between the Hugoniot and Birch-Murnaghan EoS formulations at high compressions [*Jeanloz*, 1989]. Similar discrepancies have been observed, for instance, in values for K_S' derived from ultrasonic and shock wave data for row 6 elements and Zr [*Steinberg*, 1982]. Figure 4a shows that the difference between the LPP Hugoniots modeled from parameters determined from either shock wave or static experiments is quite small in P-ρ space at ~40 GPa.

[20] There are no previous Hugoniot data for wadsleyite, so we must reference our result to static data in order to map out the low-pressure phase regime. For ρ_o = 3.47 Mg/m^3, K_{oS} = 172 ± 2 Gpa, and K_S' = 4.2 ± 0.1 [*Li et al.*, 2001], the LPP Hugoniot of fully dense wadsleyite would be U_S = 7.08 km/s + 1.35 u_p. However, the average initial density of our samples is 3.412 Mg/m^3 (lower than the theoretical density for wadsleyite, 3.47 Mg/m^3), so we apply a Mie-Grüneisen correction (see section 3.3, equation 8) using

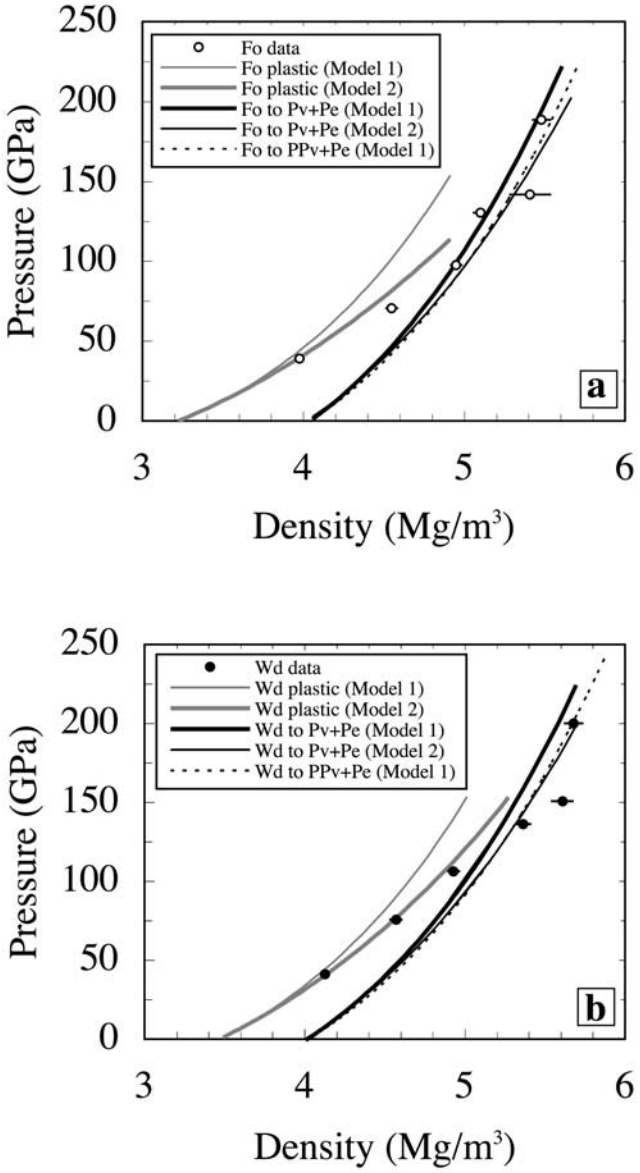

Figure 4. Model Hugoniots for candidate phases, calculated using the different model parameters outlined in Table 2. (a) Pressure versus density for forsterite (Fo) shown with model Hugoniots for Fo (models 1 and 2, corresponding to K' = 4.44 and K' = 3.25, respectively), Fo transformed to Pv + Pe (models 1 and 2), and Fo transformed to PPv + Pe (model 1 only; model 2 is not distinguishable at this scale). Model Hugoniots for Fo transformed to a high-pressure melt not shown. (b) Pressure versus density for wadsleyite, shown with model Hugoniots for Wd (models 1 and 2, corresponding to K = 4.2 and K = 3.25, respectively), Wd transformed to Pv + Pe (models 1 and 2), and Wd transformed to PPv + Pe (model 1 only). Model Hugoniots for Wd transformed to a high-pressure melt not shown.

Table 2. Parameters for Model Hugoniot Calculations[a]

Phase	Model	ρ_0, Mg/m^3	K_{oS}, GPa	K'	γ_0	q	E_{tr}, J/kg	Data Sources and Notes
Fo	1	3.222	128.4	4.44	nd	nd	0	*Li et al.* [1998] ultrasonic data
	2	3.222	132.9	3.25	nd	nd	0	Fitted to LPP shock wave data of *Syono et al.* [1981a] and *McQueen* [1968]
Wd	1	3.470	172.0	4.20	1.32	1.00	212,000	*Li et al.* [1998] ultrasonic data; E_{tr} from *Jacobs and Oonk* [2001]; γ_0 *and q from Kiefer et al.* [2001]
	2	3.470	172.0	3.25	1.32	1.00	212,000	By analogy to forsterite LPP shock fit; see text
Pe	1	3.584	160.3	4.13	1.52	1.00		*Fei et al.* [1990]
	2	3.584	152.6	4.49	1.37	0.94		(D. Sun et al., manuscript in preparation, 2007): global fit to shock and static data of *Vassiliou and Ahrens* [1981], *Svendsen and Ahrens* [1987], *Duffy and Ahrens* [1995], *Dewaele et al.* [2000], and *Speziale et al.* [2001]
Pv	1	4.108	252.8	4.34	1.81	1.39		This work, fit to the works of *Vanpeteghem et al.* [2006], *Li & Zhang* [2005], *Fiquet et al.* [1998], *Saxena et al.* [1999], and *Funamori et al.* [1996]
	2	4.108	254.0	3.98	1.30	1.70		This work, fit to the works of *Vanpeteghem et al.* [2006], *Fiquet et al.* [1998], *Fiquet et al.* [2000], and *Funamori et al.* [1996]
PPv	1	4.071	215.9	4.41	1.68	1.31		*Tsuchiya et al.* [2005]
	2	4.094	231.9	4.43	1.55	0.91		*Oganov and Ono* [2004]
Pe + Pv	1	3.943	218.7	4.27	1.71	1.25	848,000	VRH average of Pe-a and Pv-a; E_{tr} from the work of *Navrotsky* [1995]
	2	3.943	216.0	4.14	1.32	1.41	848,000	VRH average of Pe-b and Pv-b; E_{tr} from the work of *Navrotsky* [1995]
Pe + PPv	1	3.919	196.6	4.32	1.63	1.20	1,037,000	VRH average of Pe-b and PPv-a; E_{tr} estimated from the work of *Tsuchiya et al.* [2005]
	2	3.934	203.2	4.45	1.49	0.92	1,037,000	VRH average of Pe-a and PPv-b; E_{tr} estimated from the work of *Tsuchiya et al.* [2005]
HPP Melt	1	3.934	84.3	3.20	1.81	−1.00	430,337	Extreme low-q acceptable fit solution
	2	3.625	114.8	2.91	1.12	−1.93	1,195,620	Central acceptable fit solution
	3	3.772	222.6	3.91	0.83	−2.90	5,656,399	Extreme high−q acceptable fit solution

[a]See text for abbreviations and explanation of HPP melt parameters.

$\gamma_o = 1.32$ and $q = 1$ [*Kiefer et al.*, 2001] to obtain a model Hugoniot. The resulting curve does not fit any of our data within error. However, if by analogy to the forsterite LPP regime we assume $K_S' = 3.25$ for wadsleyite, then the resulting model LPP Hugoniot for initial wadsleyite with bulk density of 3.412 fits both the 41 and 76 GPa data for wadsleyite. The 106 GPa datum on wadsleyite is only slightly below this LPP Hugoniot. We interpret this as evidence that the low-pressure phase persists to substantially higher pressure on the wadsleyite Hugoniot compared with the forsterite Hugoniot, because of lower shock temperatures and hence more sluggish transformation kinetics. However, a final interpretation of the LPP regime on the wadsleyite Hugoniot depends on resolving the discrepancy in apparent K_S' between shock wave and static compression data.

4.1.2. Mixed-Phase Regime

[21] *Syono et al.* [1981a] proposed that a "mixed-phase regime" exists for single-crystal forsterite shocked to pressures between 50 and 120 GPa and that this regime exists over a smaller pressure range for polycrystalline forsterite (best seen in U_s-u_p space, in the work of *Syono et al.* [1981a], Figure 2). Examination of the literature data (Figure 1), however, reveals a lack of data for single crystals between ~60 and 80 GPa and, as already mentioned, considerable scatter in the data at higher pressures. Therefore precise delineation of the MP regime for single crystals is not possible based on available data. Moreover, the nature of the MP regime is not well understood. On the basis of recovery experiments conducted up to 75 GPa, *Jeanloz* [1980] argued that no reconstructive transformation actually occurs within this region but that a variety of compression mechanisms of the olivine structure could be invoked to explain the Hugoniot data. However, later experiments performed to higher pressures by *Syono et al.* [1981b] recovered samples showing partial breakdown of forsterite to MgO plus a glassy phase with a composition close to $MgSiO_3$ considered to represent former perovskite. Furthermore, *Syono et al.* [1981b] pointed out that the peak temperatures in recovery experiments are significantly lower than in Hugoniot EoS experiments, necessitating higher equivalent pressures to drive transformation. It therefore appears reasonable that the MP region on the Hugoniot in fact represents a region of partial transformation to the high-pressure assemblage. We propose that our data at ~71 GPa for forsterite and at 106 GPa for wadsleyite are in the MP regime; like the metastable LPP regime, the MP regime is expected to extend to higher pressure for wadsleyite because of the colder temperatures reached along the Hugoniot. We note again, as discussed above, that the data at 40 GPa for forsterite and at 41 and 76 GPa for wadsleyite may also be in the MP regime if the static measurements of K' are used to define the LPP Hugoniot.

4.1.3. High-Pressure Phase Regime

[22] We interpret the data at 97 and 130 GPa for forsterite and 136 GPa for wadsleyite to represent solid-state HPP regimes. This case can be made more strongly for the forsterite data because with two data points, we can observe the slope of the Hugoniot in this interval and document that it is much steeper than in the MP regime, consistent with compression of a constant phase assemblage rather than with progressive transformation to denser structures. For wadsleyite, we have only one data point in this regime, and therefore the conclusion that it is a HPP rather than MP regime is based on reference to model HPP Hugoniots, as discussed below.

[23] *Jackson and Ahrens* [1979] proposed that their data on forsterite from 120 to 165 GPa reflect complete transformation to the high-pressure assemblage Pe + Pv. A puzzling issue is that later experiments by *Watt and Ahrens* [1983] demonstrated a strong influence of crystallographic orientation on the Hugoniot, with crystals shocked along the *a* and *c* axes reaching lower density shock states than those shocked by *Jackson and Ahrens* [1979] along the *b* axes. However, such crystallographic dependence was not seen in Fo90 olivine single crystals shocked to similar pressures [*Furnish and Brown*, 1986] or in enstatite single crystals [*Akins et al.*, 2004]. Taken together, the Hugoniot data on single-crystal Fo at pressures of 120 GPa and above show extreme scatter (Figure 1), presenting considerable difficulty for accurately defining the high-pressure phase segment of the Hugoniot.

[24] Our data define a HPP regime with a significantly stiffer Hugoniot than that proposed by *Jackson and Ahrens* [1979]. From a fit to the forsterite data at 97 and 130 GPa (segment 4f in Figure 3), we obtain

$$U_S(\mathrm{km/s}) = (2.57 \pm 0.93) + (2.04 \pm 0.27)u_p$$

(note that the uncertainty in the slope and intercept of this fit are correlated; in the u_p range defined by the data, the uncertainty in U_s is only ~0.1 km/s).

[25] We interpret this data by calculating the theoretical Hugoniots (Figures 3 and 4) for conversion from forsterite to various high-pressure assemblages using the equations given in section 3 and the parameters listed in Table 2. Properties of multiphase assemblages are calculated from single-phase properties at ambient pressure using Voigt-Reuss-Hill (VRH) averaging [e.g., *Stacey*, 1998] to obtain bulk properties.

[26] The prediction of HPP Hugoniots depends on the selection of parameters defining possible high-pressure phases. We present multiple sets of parameters for these phases to reflect the uncertainty in our modeling. For periclase, we use both the model of *Fei et al.* [1990] and a more recent, global fit to static and shock wave data by (D. Sun et al., manuscript in preparation, 2007). For the post-perovskite (PPv) phase of $MgSiO_3$, we must use the density functional theory calculations of *Oganov and Ono* [2004] or *Tsuchiya et al.* [2005], since experimental data cover an insufficient pressure range to define the thermal EOS of this phase. For $MgSiO_3$ perovskite, there is unfortunately considerable disagreement among published static EoS and ultrasonic data, so we derive two sets of parameters from two approximately self-consistent subsets of the literature data. The first set of parameters considers *P-V-T* data from the work of *Funamori et al.* [1996], *Fiquet et al.* [1998], *Saxena et al.* [1999], and *Vanpeteghem et al.* [2006] and simultaneous XRD and ultrasonic data from the work of *Li and Zhang* [2005]. Notably, this fit has $K' = 4.34$ and is clearly inconsistent with the data of *Fiquet et al.* [2000]. The second set of parameters considers data from the work

of *Funamori et al.* [1996], *Fiquet et al.* [1998], *Fiquet et al.* [2000], and *Vanpeteghem et al.* [2006]. It yields $K' = 3.98$ and is clearly inconsistent with the data of *Saxena et al.* [1999] and *Li and Zhang* [2005]. We find that this fit yields densities at high pressure higher than those determined for PPv by *Murakami et al.* [2004], whose data define a density increase for the Pv-PPv transition. The second set of parameters and calculations based on it are presented here to reflect the uncertainty in our modeling exercise that results from discrepant literature data, but we prefer the first set of parameters for Pv and emphasize the interpretation based on this set.

[27] We find that the HPP segment of the forsterite Hugoniot is consistent with the assemblage Pe + Pv within the errors of the data and the first set of Pe + Pv model parameters (Figure 4). The Hugoniot of wadsleyite, on the other hand, contains no data points consistent with the assemblage Pe + Pv, assuming the first set of Pe + Pv model parameters. Although the wadsleyite data point at 136 GPa can be reconciled with the assemblage Pe + Pv using the second set of Pe + Pv model parameters, this leaves us with no acceptable interpretation for the HPP segment of the forsterite Hugoniot. Instead, we prefer the interpretation that the wadsleyite data point at 136 GPa represents an assemblage of Pe + PPv. The estimated shock temperature for this data point (3600 K; calculated using equations 10 and 11) is indeed in the stability field of PPv + Pe [*Murakami et al.*, 2004], whereas the forsterite data are at higher temperature, in the perovskite + MgO stability field or its superheated metastable extension. To our knowledge, this is the first inference of PPv in a shock wave experiment.

4.1.4. Melt Regime

[28] The density increases by 6.0 ± 2.7% on the forsterite Hugoniot between 130 and 142 GPa and by 4.6 ± 1.6% on the wadsleyite Hugoniot between 136 and 151 GPa. We argue that the large density increases in this range result from melting. The densities obtained at 142 GPa for forsterite and at 151 GPa for wadsleyite are denser than the prediction for Pe + PPv (Figure 4), which is the densest known solid phase assemblage in this system. Similar density increases upon melting have been observed on the Hugoniots of quartz, cristobalite, enstatite, and enstatite glass [*Akins and Ahrens*, 2002; *Akins et al.*, 2004], where additional information such as shock temperature and sound velocity measurements constrains the interpretation that melting of these silicates at high shock pressures occurs with increases in density.

[29] The density increases along the Hugoniots cannot be directly interpreted as density differences across the high-pressure melting curve until two corrections are made. First, the expected compression of the HPP phase assemblage must be accounted for to yield comparisons of volume at equal pressure. Second, the states inferred along the high-pressure solid and melt Hugoniots at the transition pressure are at different temperatures and a correction for thermal expansion of the HPP solid assemblage is required [*Akins et al.*, 2004].

[30] First, we extrapolate the HPP solid Hugoniot densities to the pressure of the first melt-regime data. The increase in density along the forsterite Hugoniot between 130 and 142 GPa is 0.309 ± 0.139 Mg/m^3. The slope of the Pe + Pv model Hugoniots in P-ρ space in this pressure range suggests an increase in density of 0.078 Mg/m^3, whereas the linear slope defined by the two HPP regime data points for forsterite suggests an increase of 0.056 Mg/m^3. Taking the average of these two estimates, the increase in Pe + Pv density is 0.067 ± 0.011 Mg/m^3 over this pressure range. This leaves a difference of 0.242 ± 0.150 Mg/m^3 (4.7 ± 2.9%) between the solid and melt Hugoniot densities for forsterite at 142 GPa. For wadsleyite, the increase in density from 136 to 151 GPa is 0.245 ± 0.086 Mg/m^3. The slopes of the two (nearly identical) Pe + PPv model Hugoniots imply an increase of 0.075 ± 0.005 Mg/m^3, leaving a difference of 0.170 ± 0.091 Mg/m^3 (3.2 ± 1.7%) between the solid and melt Hugoniot densities for wadsleyite at 151 GPa.

[31] Next, we estimate what fraction of the observed density increase is due to thermal expansion and the temperature difference between solid and melt Hugoniot states. Properties of the unknown high-pressure melt phase (see below) needed to estimate shock temperature are derived by fitting the data; we consider that structural changes with compression in the melt make it unreasonable to try to fit the HPP melt data with the properties of forsterite liquid at ambient pressure (see *Akins et al.* [2004]). For shock temperature estimates in the Pe + Pv, Pe + PPv, and melt regimes, we employ equations (10) and (11) and assume a constant heat capacity C_v of $3nR$ = 1240 J/kg, where $n = 7$ is the number of atoms per formula unit and R is the universal gas constant. Model shock temperatures for the solid assemblages at the pressure of the first point on the Hugoniot interpreted as melt are 750–1100 K higher than the corresponding model shock temperatures for the melt, and thermal expansion coefficients of Pe + Pv or Pe + PPv at 142–151 GPa (estimated from $(\partial V / \partial T)_P = \gamma C_V / K_T$) are $1 \pm 0.1 \times 10^{-5}$ [cf. *Stacey*, 1998]. This leads to a difference of 1.0 ± 0.2% (absolute) between the observed density difference and the estimated equilibrium density change on melting. Combining this difference with the extrapolation of the Hugoniots outlined above, we find that the high-pressure melt of Mg_2SiO_4 composition is 3.7 ± 3.0% denser than Pe + Pv at 142 GPa and 2.2 ± 1.8% denser than Pe + PPv at 151 GPa. These formal uncertainties taken separately suggest that this result is marginally significant for either the forsterite or wadsleyite data independently, but the agreement between the density increases observed upon melting on both Hugoniots provides confidence that the melt is in fact denser than the solids.

4.2. Grüneisen Parameter of Mg_2SiO_4 Liquid

[32] The internal energies (E) of the Hugoniot states are calculated according to equation (3) [e.g., *Ahrens*, 1987]. On the basis of the energy and pressure difference between the two inferred melt Hugoniots, we can estimate the Grüneisen parameter (γ) of high-pressure melt of Mg_2SiO_4 composition, assuming the Mie-Grüneisen EoS ($\gamma(V) = V(\Delta P / \Delta E)_v$) and taking into account the transition energy between forsterite and wadsleyite at ambient conditions (constrained by calorimetry to 2.1×10^5 J/kg; [*Jacobs and Oonk*, 2001]). The solid line in Figure 5 shows this calculation of γ as a function of density, determined from the difference between the two Hugoniot curves (constrained by two data points for forsterite and two for wadsleyite) and plotted within the density range of the melt-phase data; the uncertainty envelope is propagated from uncertainties in all the input data and parameters.

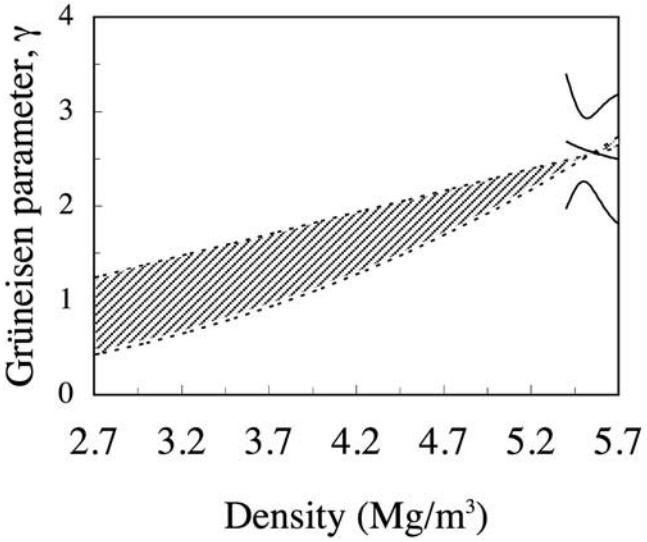

Figure 5. Grüneisen parameter (γ) of Mg_2SiO_4 liquid versus density. Heavy solid line shows result from differential analysis of ΔE and ΔP between the melt-phase forsterite and wadsleyite Hugoniot data within the density range sampled by the experiments (1σ uncertainty envelope for this function shown by light solid lines). Hashed-line envelope (within the dashed lines) shows the range of best fitting γ functions derived from an overall fit of the EoS of HPP melt to the absolute positions of the melt-phase Hugoniot data, extrapolated to ambient pressure (see Table 2 for parameters derived from fitting).

The best fit values of γ are nearly constant in this range, decreasing from 2.68 to 2.49 with increasing density from 5.4 to 5.7 Mg/m^3. A similarly high value, $\gamma = 2.1$, was derived by *Brown et al.* [1987b] for Fo90 olivine shocked into the melt regime at 168 GPa, on the basis of sound velocity measurements.

[33] The errors on the differential calculation shown in Figure 5 allow for the value of γ to increase, decrease, or remain constant with increasing density within the range sampled by our data points. However, 2.58 ± 0.1 is a very large value for γ of a silicate liquid at ambient conditions. For example, the γ of Mg_2SiO_4 liquid at its 1 atmosphere liquidus temperature, estimated from partial molar volume and thermal expansion data [*Lange and Carmichael*, 1990], compressibility data [*Ghiorso et al.*, 2002], and heat capacity data [*Lange and Navrotsky*, 1992], is 0.51 (thermodynamic identities needed for this calculation are in the work of *Poirier* [2000], section 2.3). This suggests that over a larger density range, γ increases with compression. Whereas the value of γ in solid phases that do not undergo phase transformations normally decreases upon compression [e.g., *Jeanloz and Roufosse*, 1982], structural changes with compression cause liquids to show the opposite behavior, with γ increasing with decreasing volume [e.g., *Stixrude and Karki*, 2005].

[34] We can also constrain the global $\gamma(V)$ function with a different treatment of our data, by fitting the "absolute" positions of the four melt-phase data on the forsterite and wadsleyite Hugoniots to a complete EoS for the HPP melt phase. We calculate theoretical Hugoniots for conversion of forsterite and wadsleyite to the model HPP melt phase and compute an error function (χ^2) from the sum of squared differences in pressure and u_p (weighted by data uncertainty) between the data and the model (evaluated at the experimental volume) for the four melt data points. Minimization of this error function yields a preferred model. Although there are too many parameters (V_o, K_o, K', γ_o, q, and E_{tr}) to uniquely define the EoS of the high-pressure melt phase from four data points, the allowable range of parameters is bounded by the data and by plausibility arguments, as illustrated in Figure 6. Since the essential point we wish to demonstrate is that the Grüneisen parameter increases with compression (i.e, $q < 0$), we show best fitting solutions as a function of fixed values of q. We only find acceptable fits ($\chi^2 < 10$) for $q < -1.0$. Fits for $q > -1.0$ have higher χ^2 values and negative transition energies from forsterite to HPP melt, which we consider unrealistic as it implies that forsterite is metastable relative to HPP melt at ambient conditions, if this parameter is unconstrained. For q in the range of -2.0 to -3.0, the value of χ^2 is acceptable but the value of E_{tr} rises steeply. The range of successful values for the $\gamma(V)$ function, referenced to an initial density of 2.7 Mg/m^3, is $0.5(V_o / V)^{-2.3}$ to $1.24(V_o / V)^{-1.0}$. This range of models is represented by the hashed-line envelope in Figure 5, and parameters corresponding to three representative models within this envelope are provided in Table 2. Importantly, we cannot obtain melt phase Hugoniots that fit our data with a constant or decreasing $\gamma(V)$ function. This result in the Mg_2SiO_4 system provides experimental verification of the behavior predicted by *Stixrude and Karki* [2005] in $MgSiO_3$. We note, however, that our data cannot constrain whether γ in the liquid increases continuously with compression, as illustrated in Figure 7. *Stixrude and Karki* [2005] observed a continuous change in thermodynamic properties in model $MgSiO_3$ liquid, attending a continuous, linear increase in mean silicon-oxygen coordination number with compression. However, many glasses and some liquids display polyamorphic or liquid-liquid phase transitions [*McMillan*, 2004], which could manifest as discontinuous jumps in γ

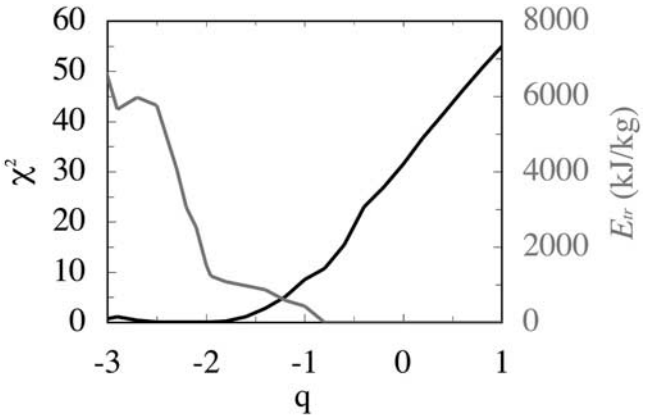

Figure 6. Sensititivity analysis of fitting HPP melt EoS to the absolute positions of the melt-phase Hugoniot data. Chi-square value (see text) and E_{tr} shown as a function of fixed value of 0. For $q > -1.0$, E_{tr} is fixed to 0 in this figure because otherwise it would converge to a negative value, which is unrealistic.

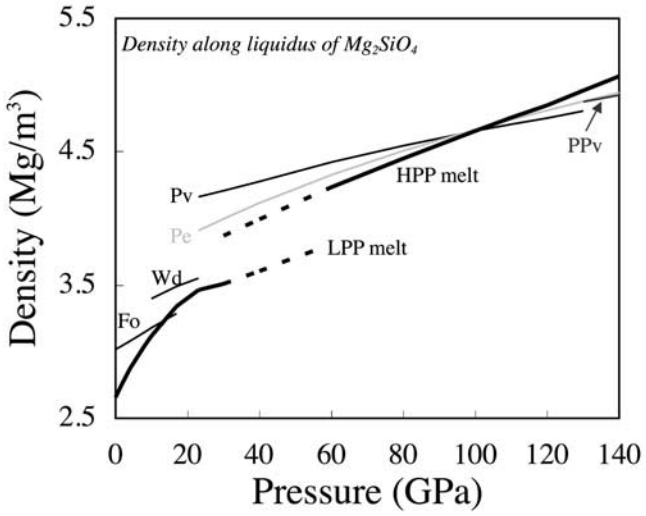

Figure 7. Density of high-pressure phases evaluated along the liquidus of Mg_2SiO_4, illustrating crossovers in density between liquid and solids.

and ρ accompanying relatively sudden coordination changes.

5. Implications

5.1. Density of Melts at the CMB

[35] The density increase upon melting observed in this study is comparable to that seen upon melting on the Hugoniot of enstatite at 170 GPa by *Akins et al.* [2004]. The similarity of these two results suggests that the presence of melt phases denser than solids in the MgO-SiO_2 system at pressures near the CMB is a robust result that applies over the entire Mg/Si range of likely mantle compositions. In Figure 7, we show the predicted density crossover for selected solids and liquid, plotted along the *P-T* curve of the liquidus of Mg_2SiO_4. The liquidus is calculated from static experimental data at low pressures [*Davis and England*, 1964; *Presnall and Walter*, 1993] and from the melting curve of *Luo et al.* [2004], on the basis of modification of the shock temperature data of *Lyzenga and Ahrens* [1980].

[36] Recently, on the basis of first-principles molecular-dynamics simulations, *Stixrude and Karki* [2005] proposed that the density under lower mantle conditions of $MgSiO_3$ liquid closely approaches that of Pv but does not exceed it. However, they pointed out that partitioning of other elements (Fe and Ca) into the melt in a real multicomponent system might be sufficient to make the liquid denser than the solid. Our present results also support the idea that melts are negatively or neutrally buoyant at pressures close to the CMB, where temperatures may be high enough to induce melting. This lends further credence to previous models calling for a dynamically stable partial melt to explain the existence of ultra-velocity zones at the base of the mantle [*Garnero and Helmberger*, 1995].

5.2. Magma Ocean Dynamics

[37] Thermodynamic identities show that an alternate definition of γ is $[\partial \ln T / \partial \ln \rho)_S$, which means that this parameter can be interpreted as the adiabatic temperature gradient with increasing density [*Miller et al.*, 1991]. Our determination of the Grüneisen parameter of Mg_2SiO_4 liquid thus provides an estimate of the temperature profile of a deep terrestrial magma ocean. This is briefly illustrated in Figure 8, which shows the liquidus of forsterite throughout the mantle pressure range (see section 5.1) and the isentropic temperature profile at the onset of first crystallization for two cases, corresponding to the conventional estimate of $\gamma = 1.5\ (V / V_o)$ [*Miller et al.*, 1991] and our new estimate of $\gamma = 0.75\ (V / V_o)^{-1.7}$. Pressure-volume along both isentropes was calculated using the third-order Birch-Murnaghan expression with $V_o = 52.054$ cc/mol [*Lange and Carmichael*, 1990] and $K_{oS} = 27$ GPa [*Ghiorso et al.*, 2002]. For the conventional γ formulation, we use $K_S' = 5$ [*Ghiorso et al.*, 2002]; in conjunction with our proposed γ function, we use $K_S' = 3.8$. The constraints on K' of the liquid are wide, but we have chosen the value so as to go through our high-pressure data. Although this formulation is strictly appropriate only for low pressures, it fits reasonably well the density predicted from molecular dynamics by *Belonoshko and Dubrovinsky* [1996] up to 135 GPa and should serve to illustrate the approximate form of the isentrope in *P-T* space.

[38] Compared to the conventional estimate [*Miller et al.*, 1991] of $q = 1$ (i.e., constant γ / V), our estimate of q leads to a temperature ~50% higher at the CMB for adiabats with equal potential temperature. This is a large enough difference to substantially influence the dynamics of a magma ocean, for instance affecting whether the magma ocean is expected to crystallize from the bottom or from the top. For the conventional estimate, the critical adiabat has a potential temperature of 2300 K, is almost parallel to the liquidus, and intersects it at the CMB. This model suggests that a whole mantle forsterite magma ocean, upon cooling, would begin to differentiate by fractionation of perovskite or

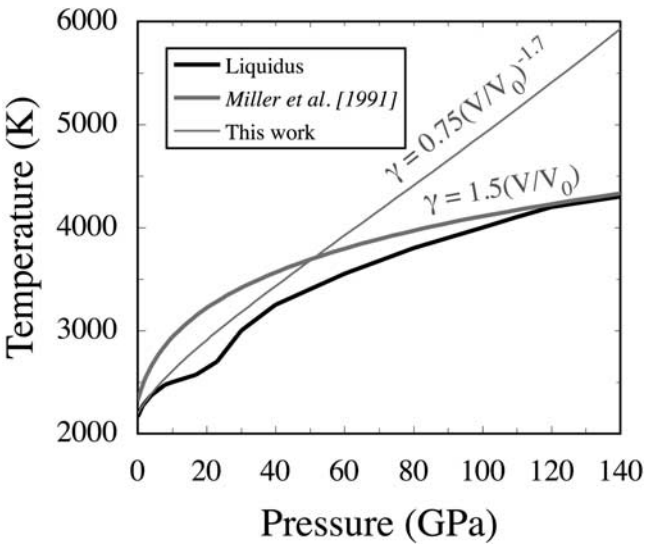

Figure 8. Comparison of liquidus of Mg_2SiO_4 (heavy black line) with isentropic temperature profiles at first onset of crystallization during cooling of a forsterite magma ocean. Two profiles shown, corresponding to $\gamma = 1.5\ (V / V_o)$ (*Miller et al.* [1991], heavy gray line) and $\gamma = 0.75\ (V / V_o)^{-1.7}$ (this work, light grey line).

periclase at the bottom. On the other hand, for our new estimate of γ, the critical adiabat has a potential temperature of 2192 K (similar to the 1 bar liquidus of forsterite), is much steeper than the liquidus, and intersects it near the surface. This model suggests that a whole mantle forsterite magma ocean would begin to differentiate by fractionation of olivine at the top or possibly majorite near the transition zone. Subsequent evolution would be modified by complicated effects including crystal flotation/sinking, change in residual liquid composition, and development of boundary layers [e.g., *Agee and Walker*, 1988; *Abe*, 1997; *Elkins-Tanton et al.*, 2005]. It is beyond the scope of this paper to construct a comprehensive magma ocean evolution model. Therefore we merely point out the dramatic effect that our measured parameters would have on the initial stages of such a model.

[39] **Acknowledgments.** This work was supported by NSF grants EAR-0207934, OCE-0241716, and OCE-0550216. We thank P. Gelle, M. Long, C. McCaughey, and R. Oliver for their expert technical support. Daoyuan Sun kindly shared his results on fitting the equation of state of MgO. The manuscript was improved by reviews from Carl Agee and an anonymous referee. Contribution no. 9155, Division of Geological and Planetary Sciences, California Institute of Technology.

References

Abe, Y. (1997), Thermal and chemical evolution of the terrestrial magma ocean, *Phys. Earth Planet. Inter.*, *100*, 27–39.

Agee, C. B., and D. Walker (1988), Mass balance and phase density constraints on early differentiation of chondritic mantle, *Earth Planet. Sci. Lett.*, *90*, 144–156.

Ahrens, T. J. (1971), Equation of state of forsterite, *J. Geophys. Res.*, *76*, 518–528.

Ahrens, T. J. (1987), Shock wave techniques for geophysics and planetary physics, in *Methods of Experimental Physics*, edited by C. G. Sammis and T. L. Henyey, pp. 182–235, Elsevier, New York.

Akins, J. A., and T. J. Ahrens (2002), Dynamic compression of SiO_2: A new interpretation, *Geophys. Res. Lett.*, *29*(10), 1394, doi:10.1029/2002GL014806.

Akins, J. A., S.-N. Luo, P. D. Asimow, and T. J. Ahrens (2004), Shock-induced melting of $MgSiO_3$ perovskite and implications for melts in Earth's lowermost mantle, *Geophys. Res. Lett.*, *31*, L14612, doi:10.1029/2004GL020237.

Andrault, D., M. A. Bouhifd, J. P. Itie, and P. Richet (1995), Compression and amorphization of (Mg,Fe)2SiO4 olivines: an X-ray diffraction study up to 70 GPa, *Phys. Chem. Miner.*, *22*, 99–107.

Belonoshko, A. B., and L. S. Dubrovinsky (1996), Molecular and lattice dynamics study of the MgO-SiO2 system using a transferable interatomic potential, *Geochim. Cosmochim. Acta*, *60*, 1645–1656.

Brown, J. M., M. D. Furnish, and D. A. Boness (1987a), Sound velocities for San Carlos olivine, in *Shock Waves in Condensed Matter—1987*, edited by S. C. Schmidt and N. C. Holmes, pp. 119–122, Elsevier, New York.

Brown, J. M., M. D. Furnish, and R. G. McQueen (1987b), Thermodynamics for (Mg, Fe)$_2SiO_4$ from the Hugoniot, in *High-Pressure Research in Mineral Physics*, edited by M. H. Manghnani and Y. Syono, pp. 373–384, AGU, Washington, D.C.

Davis, B. T. C., and J. L. England (1964), The melting of forsterite up to 50 kilobars, *J. Geophys. Res.*, *69*, 1113–1116.

Dewaele, A., G. Fiquet, D. Andrault, and D. Hausermann (2000), P-V-T equation of state of periclase from synchrotron radiation measurements, *J. Geophys. Res.*, *105*, 2869–2877.

Downs, R. T., C.-S. Zha, T. S. Duffy, and L. W. Finger (1996), Elasticity of forsterite to 17.2 GPa and effects of pressure media, *Am. Mineral.*, *81*, 51–55.

Duffy, T. S., and T. J. Ahrens (1995), Compressional sound-velocity, equation of state, and constitutive response of shock-compressed magnesium-oxide, *J. Geophys. Res.*, *100*, 529–542.

Duffy, T. S., C.-S. Zha, R. T. Downs, H.-K. Mao, and R. J. Hemley (1995), Elasticity of forsterite to 16 GPa and the composition of the upper mantle, *Nature*, *378*, 170–173.

Elkins-Tanton, L. T., P. C. Hess, and E. M. Parmentier (2005), Possible formation of ancient crust on Mars through magma ocean processes, *J. Geophys. Res.*, *110*, E12501, doi:10.1029/2005JE002480.

Farver, J. R., R. A. Yund, and D. C. Rubie (1994), Magnesium grain boundary diffusion in forsterite aggregates at 1000°–1300°C and 0.1 MPa to 10 GPa, *J. Geophys. Res.*, *9*, 19809–19819.

Fei, Y., S. K. Saxena, and A. Navrotsky (1990), Internally consistent thermodynamic data and equilibrium phase relations for compounds in the system MgO-SiO_2 at high pressure and high temperature, *J. Geophys. Res.*, *95*, 6915–6928.

Fei, Y., J. Van Orman, J. Li, W. van Westrenen, C. Sanloup, W. Minarik, K. Hirose, T. Komabayashi, M. Walter, and K. Funakoshi (2004), Experimentally determined postspinel transformation boundary in Mg_2SiO_4 using MgO as an internal pressure standard and its geophysical implications, *J. Geophys. Res.*, *109*, B02305, doi:10.1029/2003JB002562.

Fiquet, G., D. Andrault, A. Dewaele, T. Charpin, M. Kunz, and D. Haüsermann (1998), P-V-T equation of state of $MgSiO_3$ perovskite, *Phys. Earth Planet. Inter.*, *105*, 21–31.

Fiquet, G., A. Dewaele, D. Andrault, M. Kunz, and T. Le Bihan (2000), Thermoelastic properties and crystal structure of $MgSiO_3$ perovskite at lower mantle pressure and temperature conditions, *Geophys. Res. Lett.*, *27*, 21–24.

Funamori, N., T. Yagi, W. Utsumi, T. Kondo, and T. Uchida (1996), Thermoelastic properties of $MgSiO_3$ perovskite determined by in situ X ray observations up to 30 GPa and 2000 K, *J. Geophys. Res.*, *101*, 8257–8269.

Furnish, M. D., and J. M. Brown (1986), Shock loading of single-crystal olivine in the 100–200 GPa range, *J. Geophys. Res.*, *91*, 4723–4729.

Garnero, E. J., and D. V. Helmberger (1995), A very slow basal layer underlying large-scale low-velocity anomalies in the lower most mantle beneath the Pacific—Evidence from core phases, *Phys. Earth Planet. Inter.*, *91*, 161–176.

Ghiorso, M. S., M. M. Hirschmann, P. W. Reiners, and V. C. Kress (2002), The pMELTS: A revision of MELTS for improved calculation of phase relations and major element partitioning related to partial melting of the mantle to 3 GPa, *Geochem. Geophys. Geosyst.*, *3*(5), 1030, doi:10.1029/2001GC000217.

Gwanmesia, G. D., B. Li, and R. C. Liebermann (1993), Hot Pressing of polycrystals of high-pressure phases of mantle minerals in multi-anvil apparatus, *J. Pure Appl. Geophys.*, *141*, 467–484.

Hixson, R. S., and J. N. Fritz (1992), Shock compression of tungsten and molybdenum, *J. Appl. Phys.*, *71*, 1721–1728.

Ito, E., and E. Takahashi (1989), Postspinel transformations in the system Mg_2SiO_4–Fe_2SiO_4 and some geophysical implications, *J. Geophys. Res.*, *94*., 10,637–10,646.

Jackson, I., and T. J. Ahrens (1979), Shock-wave compression of single crystal forsterite, *J. Geophys. Res.*, *84*, 3039–3048.

Jacobs, M. H. G., and H. A. J. Oonk (2001), The Gibbs energy formulation of the a, b and g forms of Mg_2SiO_4 using Grover, Getting and Kennedy's empirical relation between volume and bulk modulus, *Phys. Chem. Miner.*, *28*, 572–585.

Jeanloz, R. (1980), Shock effects in olivine and implications for Hugoniot data, *J. Geophys. Res.*, *85*, 3163–3176.

Jeanloz, R. (1989), Shock wave equation of state and finite strain theory, *J. Geophys. Res.*, *94*, 5873–5886.

Jeanloz, R., and M. Roufosse (1982), Anharmonic properties: ionic model of the effects of compression and coordination change, *J. Geophys. Res.*, *87*, 10,763–10,772.

Kiefer, B., L. Stixrude, J. Hafner, and G. Kresse (2001), Structure and elasticity of wadsleyite at high pressures, *Am. Mineral.*, *86*, 1387–1395.

Knittle, E., and R. Jeanloz (1987), Synthesis and equation of state of (Mg,Fe)SiO_3 perovskite to over 100 gigapascals, *Science*, *235*, 668–670.

Kubo, T., E. Ohtani, and K.-I. Funakoshi (2004), Nucleation and growth kinetics of the a-b transformation in Mg_2SiO_4 determined by in situ synchrotron powder X-ray diffraction, *Am. Mineral.*, *89*, 285–293.

Lange, R. A., and I. S. E. Carmichael (1990), Thermodynamic properties of silicate liquids with an emphasis on density, thermal expansion and compressibility, in *Modern Methods of Igneous Petrology*, edited by J. Nicholls and K. Russell, pp. 25–64, Mineralogical Society of America.

Lange, R. A., and A. Navrotsky (1992), Heat capacities of Fe_2O_3-bearing silicate liquids, *Contrib. Mineral. Petrol.*, *110*, 311–320.

Li, B., and J. Zhang (2005), Pressure and temperature dependence of elastic wave velocity of $MgSiO_3$ perovskite and the composition of the lower mantle, *Phys. Earth Planet. Inter.*, *151*, 143–154.

Li, B., R. C. Liebermann, and D. J. Weidner (1998), Elastic moduli of wadsleyite (β-Mg_2SiO_4 to 7 gigapascals and 873 kelvin, *Science*, *281*, 675–677.

Li, B., R. C. Liebermann, and D. J. Weidner (2001), P-V-Vp-Vs-T measurements on wadsleyite to 7 GPa and 873 K: implications for the 410-km discontinuity, *J. Geophys. Res.*, *106*, 30,575–530,591.

Luo, S.-N., J. L. Mosenfelder, P. D. Asimow, and T. J. Ahrens (2002), Direct shock wave loading of Stishovite to 235 GPa: Implications for

perovskite stability relative to an oxide assemblage at lower mantle conditions, *Geophys. Res. Lett.*, *29*(14), 1691, doi:10.1029/2002GL015627.
Luo, S.-N., J. A. Akins, T. J. Ahrens, and P. D. Asimow (2004), Shock-compressed $MgSiO_3$ glass, enstatite, olivine, and quartz: optical emission, temperatures, and melting, *J. Geophys. Res.*, *109*, B05205, doi:10.1029/2003JB002860.
Lyzenga, G. A., and T. J. Ahrens (1980), Shock temperature measurements in Mg_2SiO_4 and SiO_2 at high pressures, *Geophys. Res. Lett.*, *7*, 141–144.
Marsh, S. P. E. (1980), LASL Shock Hugoniot Data, 658 pp. University of Calif. Press, Berkeley.
McMillan, P. F. (2004), Polyamorphic transformations in liquids and glasses, *J. Mater. Chem.*, *14*, 1506–1512.
McQueen, R. G. (1968), Shock-wave data and equations of state, in *Seismic Coupling, Advanced Research Project Agency Meeting*, edited by G. Simmons, pp. 53–106. National Technical Information Service, Springfield, Va.
Miller, G. H., E. M. Stolper, and T. J. Ahrens (1991), The equation of state of a molten komatiite 2. Application to komatiite petrogenesis and the Hadean mantle, *J. Geophys. Res.*, *96*, 11,849–811,864.
Mitchell, A. C., and W. J. Nellis (1981a), Diagnostic system of the Lawrence Livermore National Laboratory two-stage light-gas gun, *Rev. Sci. Instrum.*, *52*, 347–359.
Mitchell, A. C., and W. J. Nellis (1981b), Shock compression of aluminum, copper, and tantalum, *J. Appl. Phys.*, *52*, 3363–3374.
Mosenfelder, J. L., F. C. Marton, C. R. Ross II, L. Kerschhofer, and D. C. Rubie (2001), Experimental constraints on the depth of olivine metastability in subducting lithosphere, *Phys. Earth Planet. Inter.*, *127*, 165–180.
Mosenfelder, J. L., N. I. Deligne, P. D. Asimow, and G. R. Rossman (2006), Hydrogen incorporation in olivine from 2–12 GPa, *Am. Mineral.*, *91*, 285–294.
Murakami, M., K. Hirose, K. Kawamura, N. Sata, and Y. Ohishi (2004), Post-perovskite transition in $MgSiO_3$, *Science*, *304*, 855–858.
Navrotsky, A. (1995), Thermodynamic properties of minerals, in *Mineral Physics and Crystallography: a Handbook of Physical Constants*, edited by T. J. Ahrens, pp. 18–28. American Geophysical Union, Washington, D.C.
Oganov, A. R., and S. Ono (2004), Theoretical and experimental evidence for a post-perovskite phase of $MgSiO_3$ in Earth's D″ layer, *Nature*, *430*, 445–448.
Poirier, J.-P. (2000), *Introduction to the Physics of the Earth's Interior*, Cambridge Univ. Press, New York.
Presnall, D. C., and M. J. Walter (1993), Melting of forsterite, Mg_2SiO_4, from 9.7 to 16.5 GPa, *J. Geophys. Res.*, *98*, 19,777–19,783.
Raikes, S. A., and T. J. Ahrens (1979), Post-shock temperatures in minerals, *Geophys. J. R. Astron. Soc.*, *58*, 717–748.
Ruoff, A. L. (1967), Linear shock-velocity-particle-velocity relationship, *J. Appl. Phys.*, *38*, 4976–4980.
Saxena, S. K., L. S. Dubrovinsky, F. Tutti, and T. Le Bihan (1999), Equation of state of $MgSiO_3$ with the perovskite structure based on experimental measurements, *Am. Mineral*, *84*, 226–232.
Shim, S.-H., T. S. Duffy, and G. Shen (2001a), The post-spinel transformation in Mg_2SiO_4 and its relation to the 660-km discontinuity, *Nature*, *411*, 571–574.
Shim, S.-H., T. S. Duffy, and G. Shen (2001b), Stability and structure of $MgSiO_3$ perovskite to 2300-kilometer depth in Earth's Mantle, *Science*, *293*, 2437–2440.
Speziale, S., C. S. Zha, T. S. Duffy, R. J. Hemley, and H. K. Mao (2001), Quasi-hydrostatic compression of magnesium oxide to 52 GPa: Implications for the pressure-volume-temperature equation of state, *J. Geophys. Res.*, *106*, 515–528.
Stacey, F. D. (1998), Thermoelasticity of a mineral composite and a reconsideration of lower mantle properties, *Phys. Earth Planet. Inter.*, *106*, 219–236.
Steinberg, D. J. (1982), Some observations regarding the pressure dependence of the bulk modulus, *J. Phys. Chem. Solids*, *43*, 1173–1175.
Stixrude, L., and B. Karki (2005), Structure and freezing of $MgSiO_3$ liquid in Earth's lower mantle, *Science*, *310*, 297–299.
Svendsen, B., and T. J. Ahrens (1987), Shock-induced temperatures of MgO, *Geophys. J. R. Astron. Soc.*, *91*, 667–691.
Syono, Y., and T. Goto (1982), Behavior of single-crystal forsterite under dynamic compression, in *High-Pressure Research in Geophysics*, edited by S. Akimoto and M. H. Manghnani, pp. 563–577. Center for Academic Publications Japan, Tokyo.
Syono, Y., T. Goto, J.-I. Sato, and H. Takei (1981a), Shock compression measurements of single-crystal forsterite in the pressure range 15–93 GPa, *J. Geophys. Res.*, *86*, 6181–6186.
Syono, Y., T. Goto, H. Takei, M. Tokonami, and K. Nobugai (1981b), Dissociation reaction in forsterite under shock compression, *Science*, *214*, 177–179.
Tsuchiya, T., J. Tsuchiya, K. Umemoto, and R. M. Wentzcovitch (2004), Elasticity of post-perovskite $MgSiO_3$, *Geophys. Res. Lett.*, *31*, L14603, doi:10.1029/2004GL020278.
Tsuchiya, J., T. Tsuchiya, and R. M. Wentzcovitch (2005), Vibrational and thermodynamic properties of $MgSiO_3$ postperovskite, *J. Geophys. Res.*, *110*, B02204, doi:10.1029/2004JB003409.
Vanpeteghem, C. B., J. Zhao, R. J. Angel, N. L. Ross, and N. Bolfan-Casanova (2006), Crystal structure and equation of state of $MgSiO_3$ perovskite, *Geophys. Res. Lett.*, *33*, L03306, doi:10.1029/2005GL024955.
Vassiliou, M. S., and T. J. Ahrens (1981), The Hugoniot equation of state of periclase to 200-GPa, *Geophys. Res. Lett.*, *8*, 729–732.
Vassiliou, M. S., and T. J. Ahrens (1982), Limited aperture light source streak photography, *Rev. Sci. Instrum.*, *53*, 108–109.
Watt, J. P., and T. J. Ahrens (1983), Shock compression of single-crystal forsterite, *J. Geophys. Res.*, *88*, 9500–9512.
Zhang, L. (1998), Single crystal hydrostatic compression of (Mg,Mn,Fe,Co)$_2SiO_4$ olivines, *Phys. Chem. Miner.*, *25*, 308–312.

T. J. Ahrens, P. D. Asimow, and J. L. Mosenfelder, Division of Geological and Planetary Sciences, California Institute of Technology, Pasadena, CA, USA. (jed@gps.caltech.edu)